Selective molecular sieving through porous graphene

Steven P. Koenig, Luda Wang, John Pellegrino and J. Scott Bunch*

Membranes act as selective barriers and play an important role in processes such as cellular compartmentalization and industrial-scale chemical and gas purification. The ideal membrane should be as thin as possible to maximize flux, mechanically robust to prevent fracture, and have well-defined pore sizes to increase selectivity. Graphene is an excellent starting point for developing size-selective membranes[1-8] because of its atomic thickness[9], high mechanical strength[10], relative inertness and impermeability to all standard gases[11-14]. However, pores that can exclude larger molecules but allow smaller molecules to pass through would have to be introduced into the material. Here, we show that ultraviolet-induced oxidative etching[15,16] can create pores in micrometre-sized graphene membranes, and the resulting membranes can be used as molecular sieves. A pressurized blister test and mechanical resonance are used to measure the transport of a range of gases (H_2, CO_2, Ar, N_2, CH_4 and SF_6) through the pores. The experimentally measured leak rate, separation factors and Raman spectrum agree well with models based on effusion through a small number of ångström-sized pores.

Suspended graphene membranes were fabricated by mechanical exfoliation of graphene over predefined 5-μm-diameter wells etched into silicon oxide[17,18]. After exfoliation, the pristine graphene flakes spanning the microcavity formed suspended membranes that were impermeable to all standard gas molecules[11] and were clamped to the silicon oxide substrate by surface forces[18]. However, gas species were able to enter and exit the microcavity through the substrate by slow diffusion.

The microcavities were filled with a desired gas species by placing the sample in a chamber pressurized with a 'charging' gas to 200 kPa above ambient pressure (Fig. 1a). Before this pressurization, the chamber was flushed with the charging gas to exclude any other species. The samples were left in the pressure chamber for 4–12 days (depending on the gas species used) to allow the internal pressure p_{int} and the external pressure p_{ext} of the microcavity to equilibrate to the charging pressure p_0. On removing the sample from the pressure chamber, the higher pressure inside the microcavity compared with the ambient atmospheric pressure caused the membrane to bulge upwards (Fig. 1b). This technique enabled the preparation of a graphene-sealed microcavity with an arbitrary gas composition at a prescribed pressure.

To measure the leak rate of gas species we used both a pressurized blister test and a mechanical resonance test[11]. The pressurized blister test was used for leak rates on the order of minutes to hours, and the mechanical resonance test was used to measure leak rates on the order of seconds to minutes. In the pressurized blister test, an atomic force microscope (AFM) was used to measure the shape of the bulged graphene membrane, which was parameterized by its maximum deflection δ (Fig. 1e). Figure 1f (black) shows the maximum deflection δ versus time t for a pristine graphene membrane pressurized to 200 kPa above atmospheric pressure with

H_2 gas. The deflection decreases slowly with time, consistent with a leak of H_2 gas through the underlying silicon oxide[11,18].

Ultraviolet-induced oxidative etching was used to introduce pores into the pristine graphene membranes[15,16,19,20] (Supplementary Section S2). The membranes pressurized with H_2 gas were exposed to ultraviolet light ($\lambda_1 = 185$ nm, $\lambda_2 = 254$ nm; Jelight Model 42 ultraviolet ozone cleaner) under ambient conditions for several minutes. A number of other etching techniques have been proposed and demonstrated for graphene[19,21-27], including oxygen plasma etching, but the ultraviolet oxidative etching used here is simple and slow enough to allow for the creation of these subnanometre-sized selective pores, as demonstrated later in this Letter. Indeed, this etching technique proved to be the only successful method for controllably introducing subnanometre pores. After the oxidative etch, δ was again measured versus t (Fig. 1e and f, red; Supplementary Section S2). The maximum deflection decreases rapidly (in several minutes rather than hours, as is the case for the unetched case) and eventually leads to a downward deflection of the membrane (Fig. 1c–f). Figure 1e shows a series of cross-sections through the centre of the membrane taken by AFM at times from 0 to 8 min, and Fig. 1g presents a three-dimensional rendering of the AFM image in Fig. 1e for $t = 0$. Here, 0 min is defined as the time at which the first AFM image is captured after removing the sample from the pressure chamber. The change in deflection, as depicted in Fig. 1c,d, results from an increase in the H_2 leak rate as a result of the etching, while significant changes in the N_2 leak rate into the microcavity from the ambient atmosphere are prevented.

The molecular selectivity of the fabricated porous graphene membrane was demonstrated by measuring the rate of change of δ with time ($-d\delta/dt$) for the same membrane pressurized with a number of different gases. Figure 2a shows δ versus t for H_2, CO_2, Ar and CH_4 before and after etching, and N_2 after etching. The N_2 leak rate before etching for this particular device was not measured, but measurements for 12 other devices located on the same flake are shown in Fig. 4 and labelled 'Pristine Avg' for comparison with the after-etch leak rate. At short times, $-d\delta/dt$ is approximately linear (Fig. 2a). This rate was plotted versus kinetic diameter[28] for all the gases, using the same membrane/microcavity shown in Fig. 1, before and after etching (Fig. 2b). After etching, there is an increase in $-d\delta/dt$ by two orders of magnitude for the H_2 and CO_2 leak rates, whereas those for Ar and CH_4 remain relatively unchanged. This suggests that the etched pores change the transport mechanism for H_2 and CO_2, but leave the transport of Ar and CH_4 nearly unchanged. As the kinetic diameter cutoff in this bilayer graphene membrane is nominally that of Ar (3.4 Å; ref. 28), this membrane will be referred to as 'Bi-3.4 Å'.

The leak rates of the various gases across the porous graphene membranes can also be measured using a mechanical resonance test. This was accomplished by measuring changes in the mechanical resonant frequency f of the membrane versus t, using an optical

Department of Mechanical Engineering, University of Colorado, Boulder, Colorado 80309, USA. *e-mail: jbunch@colorado.edu
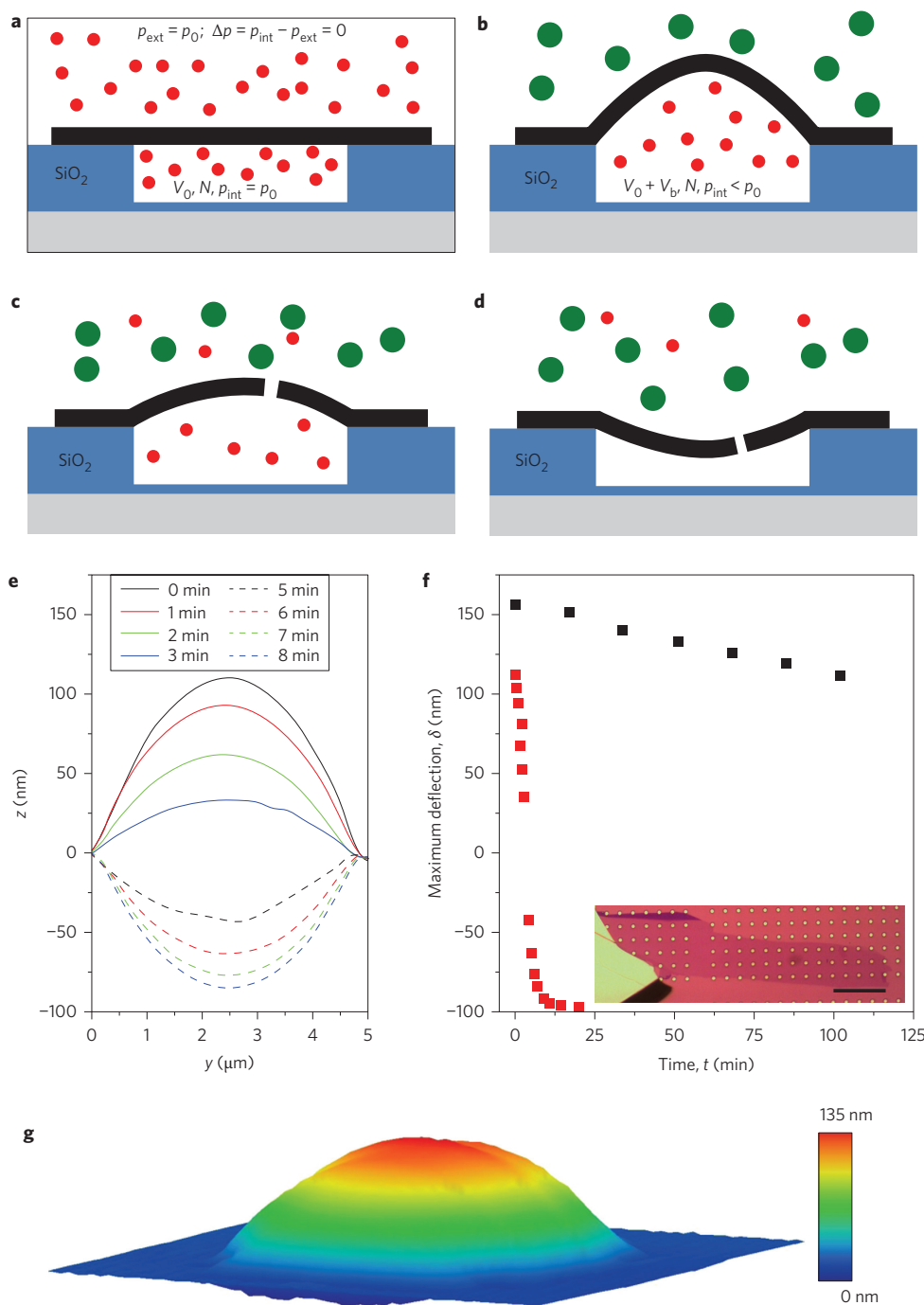
Figure 1 | Measuring leak rates in porous graphene membranes. a, Schematic of a microscopic graphene membrane on a silicon oxide substrate. We start with pristine graphene fabricated by exfoliation and fill the microchamber with 200 kPa of H_2 (represented as red circles) in a pressure chamber. Equilibrium is reached ($p_{int} = p_{ext}$) by diffusion through the silicon oxide. **b**, After removing the graphene membrane from the pressure chamber the membrane bulges upwards. We calculate p_{int} using the ideal gas law and assuming isothermal expansion. The hydrogen molecules slowly leak out of the microchamber through the silicon oxide substrate. **c**, Following etching pore(s) in the graphene membrane bigger than H_2, the H_2 is able to rapidly leak out of the microchamber through the membrane pore(s). If the pore(s) are smaller than the air molecules (mostly N_2 and O_2, denoted as green circles), air will be blocked from entering the microchamber, causing the deflection of the graphene membrane to continue to decrease until all of the H_2 molecules have exited the microchamber. **d**, Once all the H_2 molecules have leaked out of the microchamber, the membrane will deflect downwards. **e**, Deflection versus position, measured from 0 min (black) to 8 min (dashed blue) after etching, corresponding to some of the red symbols in **f**. **f**, Maximum deflection δ versus t for one membrane separating H_2 from air, measured by AFM. Black symbols represent the H_2 leak rate before etching and red symbols the H_2 leak rate after introducing selective pores into the graphene. Inset: optical image of the bilayer graphene flake used in this study, which covers many cavities in the silicon oxide substrate (scale bar is 60 μm). **g**, Three-dimensional rendering of an AFM image corresponding to the line cut at $t = 0$ in **e**.

drive and detection system that was previously used to measure mechanical resonance in suspended graphene resonators[11,29]. A pressure difference applied across the membrane leads to a pressure-induced tensioning of the membrane, which increases f for the stretched membrane. If the gas molecules introduced external to an initially evacuated microcavity can leak through the
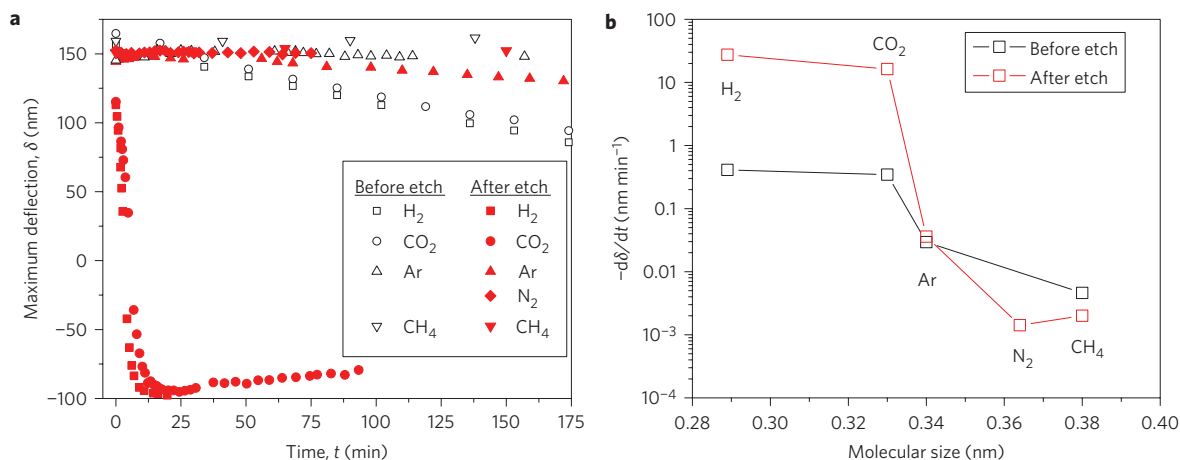
Figure 2 | Comparison of leak rates of pristine and porous graphene membranes. a, Maximum deflection δ versus t before and after etching. **b**, Average $-d\delta/dt$ versus molecular size found from the slopes of membrane deflection versus t (in **a**) before and after introducing pores into the same graphene membrane. The connecting lines show the measurements before (black) and after (red) etching.

membrane, the gas will pass through and reduce the tension in the membrane, thus decreasing f. If the gas molecules cannot leak through the membrane, f stays constant. An example of this is shown in Fig. 3. In this case, an etched porous graphene membrane was placed in a vacuum of 0.1 torr for several days to ensure the microcavity had equilibrated to the pressure of the vacuum chamber. A pure gas species was then introduced into the vacuum chamber at a given pressure (~100 torr for the case described in the main panel of Fig. 3 and ~80 torr for the inset of Fig. 3) and the resonant frequency was measured. The resonant frequency decreases with time, and from the rate of decrease, the leak rate through the porous graphene membrane can be determined. We could not observe the frequency return back to its original value because of significant gas damping when $\Delta p \approx 0$ (Supplementary Section S4). As can be seen from Fig. 3, the leak rates of H_2, CO_2, N_2 and CH_4 were found to be several seconds; however, SF_6 shows no significant change in resonant frequency over the several minutes measured. This membrane will be referred to as 'Bi-4.9 Å', as it is a bilayer membrane with the nominal sieving kinetic diameter of SF_6 (4.9 Å; ref. 28).

We derived the following expression for molecular flux, dn/dt, out of the pressurized 'blister' microcavity using the ideal gas law and Hencky's solution for a clamped circular membrane[30] (see Supplementary Section S3 for the derivation):

$$\frac{dn}{dt} = \frac{3K(\nu)(Ew\delta^2)/a^4 \cdot V(\delta) + P(C(\nu)\pi a^2)]}{RT} \cdot \frac{d\delta}{dt}$$

where a is the radius of the membrane, E is Young's modulus, w is the thickness of the membrane, R is the molar gas constant, T is temperature, $V(\delta)$ is the total volume of the microcavity in the bulged state, and $C(\nu)$ and $K(\nu)$ are geometric coefficients that depend on Poisson's ratio ν for the membrane. For the case of graphene, Young's modulus and Poisson's ratio are $E = 1$ TPa and $\nu = 0.16$, respectively, and the thickness per layer is 0.34 nm (refs 10,11,18,31). Using $\nu = 0.16$ gives coefficients of $K(\nu = 0.16) = 3.09$ and $C(\nu = 0.16) = 0.524$ (ref. 17). Figure 4 shows the normalized dn/dt (normalized to the partial pressure difference across the membrane) for the Bi-3.4 Å membrane before (black squares) and after (red squares) ultraviolet etching. Also shown is the average normalized dn/dt for 24 different unetched (12 for the case of N_2) membranes on the same graphene flake shown in the inset to Fig. 1f containing Bi-3.4 Å (black circles). Similarly, a mechanical deflection analysis allows dn/dt to be calculated from the linear approximation of the rate of frequency decay, df/dt (see

Supplementary Section S4 for details). The leak rate versus molecular size for the Bi-4.9 Å membrane is shown in Fig. 4 (red diamonds).

The changes in leak rate associated with ultraviolet etching are consistent with the introduction of a pore(s) that allows size-selective permeation of gas molecules. For the Bi-3.4 Å membrane in Fig. 2, the selectivity between CO_2 and Ar suggests that the pore(s) size(s) introduced into the graphene membrane are comparable to the kinetic diameter of Ar (3.4 Å)[28] and that the porous graphene is sieving molecules above and below this size. Similarly, for the Bi-4.9 Å membrane in Fig. 3, there are probably pore(s) larger in size than those of the Bi-3.4 Å membrane, because effective molecular sieving is seen for molecules smaller than SF_6 (4.9 Å compared with 3.8 Å for CH_4)[28]. Owing to the fact that there is probably only a small density of pores in the 5-μm-diameter membranes, imaging of the pore is not possible (Supplementary Section S2). However, the small density of pores is supported by Raman spectroscopy of the etched membranes (Supplementary Section S1).
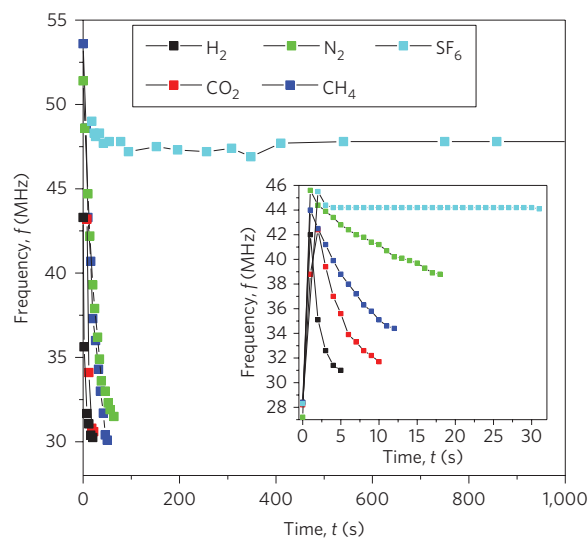

Figure 3 | Measuring leak rates in a porous graphene membrane using mechanical resonance. Frequency f versus t for H_2, CO_2, N_2, CH_4 and SF_6, with a pressure of 100 torr (~13.3 kPa) introduced into the vacuum chamber. Inset: data from the same device with 80 torr (~10.7 kPa) pressure.
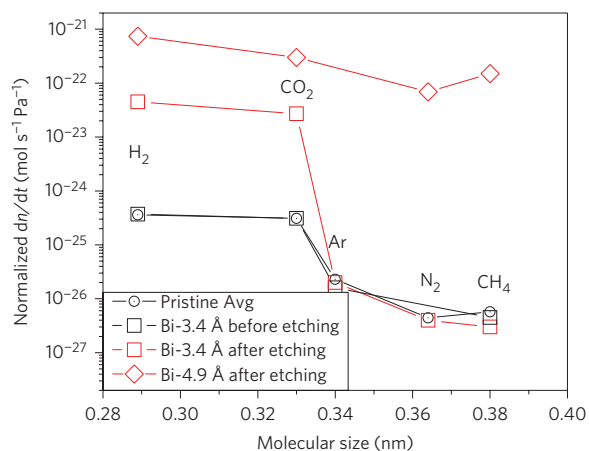
Figure 4 | Compilation of measured leak rates. Leak rates out of the microcavity for the Bi-3.4 Å membrane before etching and after etching, the Bi-4.9 Å membrane after etching, and the average before etching of 24 membranes (12 for N_2) on the same graphene flake as Bi-3.4 Å membrane (note that these last symbols are hidden by black squares for several gases.).

The measured gas leak rates can be compared to the results of computational modelling by Jiang *et al.*[1] and Blankenburg *et al.*[5]. Following the work of Jiang *et al.*[1], we estimate a H_2 leak rate on the order of $\sim 1 \times 10^{-20}$ mol s^{-1} Pa^{-1} for a hydrogen-passivated pore in graphene consisting of two missing benzene rings at room temperature (Supplementary Section S6). For the work of Blankenburg *et al.*, the H_2 leak rate was calculated to be on the order of $\sim 1 \times 10^{-23}$ mol s^{-1} Pa^{-1} through a smaller hydrogen-terminated pore consisting of a single missing benzene ring[5].

Our measured H_2 leak rate on Bi-3.4 Å was $\sim 4.5 \times 10^{-23}$ mol s^{-1} Pa^{-1}. This value is several orders of magnitude lower than Jiang *et al.*, suggesting our pores have an overall higher energy barrier for H_2 (and other species) than in their calculations. The similarity between our H_2 leak rate and that modelled by Blankenburg *et al.* suggests a similar H_2 energy barrier in our pore. However, we do not match their calculated H_2/CO_2 selectivity (2 versus $\sim 1 \times 10^{17}$). This suggests that having a bilayer graphene membrane with different chemical pore temination from the oxidative etching can be quite important.

We can also compare the measured H_2 and CO_2 leak rates in the Bi-3.4 Å and Bi-4.9 Å membranes (Fig. 4). The membrane with smaller pore size, Bi-3.4 Å (red squares), has H_2 and CO_2 leak rates (in units of 10^{-23} mol s^{-1} Pa^{-1}) of 4.5 and 2.7, respectively, compared with H_2 and CO_2 leak rates (same units) of 75 and 25, respectively, for the membrane with larger pores (red diamonds). The closeness of the magnitudes of these two values, as well as the magnitudes calculated in the cited modelling, suggests in both cases that a low density of size-selective pores are participating in the transport across the graphene membrane, and the faster leak rate for the Bi-4.9 Å membrane is consistent with having larger pores (and/or lower diffusional energy barriers) than the Bi-3.4 Å membrane. This is also consistent with the rapid effusion of gas expected from the $\sim\mu m^3$ confined volume of gas in the porous graphene sealed microchamber[11].

Both graphene membranes examined here were bilayer graphene membranes. These were selected because of the more controlled etching and increased stability of pores in bilayer graphene membranes when compared with monolayer membranes. This is consistent with previous results showing slower etching for bilayer graphene[19]. However, we also observed similar results on monolayer graphene membranes (Supplementary Section S5).

In conclusion, we have demonstrated selective molecular sieving using porous, micrometre-sized, atomically thin graphene

membranes. Pores were introduced in graphene by ultraviolet-induced oxidative etching and the molecular transport through them was measured using both a pressurized blister test and mechanical resonance. Our results are consistent with theoretical models in the literature based on effusion through ångstrom-sized pores[1,5]. The results presented here are an experimental realization of graphene gas separation membranes by molecular sieving, and represent an important step towards the realization of macroscopic, size-selective porous graphene membranes. The approach used here can also be used to probe the fundamental limits of gas transport by effusion through ångstrom-sized pores with atomic-sized channel lengths.

Methods

Suspended graphene membranes were fabricated by a combination of standard photolithography and mechanical exfoliation of graphene. An array of circles with diameters of 5 μm and 7 μm were defined by photolithography on an oxidized silicon wafer with a silicon oxide thickness of 285 nm. Reactive ion etching was then used to etch the circles into cylindrical cavities with a depth of 250–500 nm, leaving a series of wells on the wafer. Mechanical exfoliation of Kish graphite using Scotch tape was then used to deposit suspended graphene sheets over the wells.

The volume of the bulged graphene was on the order of the initial volume of the microcavity[17], and we deduced an initial $\Delta p = p_{int} - p_{ext}$ across the membrane using the ideal gas law and the isothermal expansion of the trapped gas with a constant number of molecules, N. This led to $p_0 V_o = p_{int}(V_o + V_b)$, where V_o is the initial volume of the well and $V_b = C(v)\pi a^2 \delta$ is the volume of the pressurized blister after the device is brought to atmospheric pressure and bulges upward. The constant $C(v = 0.16) = 0.524$ was determined from Hencky's solution. AFM scans were then taken continuously to deduce the leak rate of molecules out of the membrane, dn/dt.

For the resonance measurements, samples were placed in a vacuum chamber at 0.1 torr for several days to ensure the microcavity reached equilibrium with the vacuum chamber. A given pressure (ranging from 80 to 100 torr) of gas was then introduced into the vacuum chamber and the frequency was measured over time. After the introduction of a gas, the chamber was evacuated until the frequency returned to its original value when no pressure difference was present (or the signal was no longer detectable due to gas damping) and the next gas was then measured. An intensity-modulated blue laser (405 nm) was used to drive the graphene membranes, and a red laser (633 nm) was used to detect the motion of the graphene.

References

1. Jiang, D., Cooper, V. R. & Dai, S. Porous graphene as the ultimate membrane for gas separation. *Nano Lett.* **9,** 4019–4024 (2009).
2. Du, H. *et al.* Separation of hydrogen and nitrogen gases with porous graphene membrane. *J. Phys. Chem. C* **115,** 23261–23266 (2011).
3. Schrier, J. Helium separation using porous graphene membranes. *J. Phys. Chem. Lett.* **1,** 2284–2287 (2010).
4. Hauser, A. W. & Schwerdtfeger, P. Nanoporous graphene membranes for efficient ³He/⁴He separation. *J. Phys. Chem. Lett.* **3,** 209–213 (2012).
5. Blankenburg, S. *et al.* Porous graphene as an atmospheric nanofilter. *Small* **6,** 2266–2271 (2010).
6. Suk, M. E. & Aluru, N. R. Water transport through ultrathin graphene. *J. Phys. Chem. Lett.* **1,** 1590–1594 (2010).
7. Schrier, J. & McClain, J. Thermally-driven isotope separation across nanoporous graphene. *Chem. Phys. Lett.* **521,** 118–124 (2012).
8. Li, Y., Zhou, Z., Shen, P. & Chen, Z. Two-dimensional polyphenylene: experimentally available porous graphene as a hydrogen purification membrane. *Chem. Commun.* **46,** 3672–3674 (2010).
9. Meyer, J. C. *et al.* The structure of suspended graphene sheets. *Nature* **446,** 60–63 (2007).
10. Lee, C., Wei, X., Kysar, J. W. & Hone, J. Measurement of the elastic properties and intrinsic strength of monolayer graphene. *Science* **321,** 385–388 (2008).
11. Bunch, J. S. *et al.* Impermeable atomic membranes from graphene sheets. *Nano Lett.* **8,** 2458–2462 (2008).
12. Nair, R. R., Wu, H. A., Jayaram, P. N., Grigorieva, I. V. & Geim, A. K. Unimpeded permeation of water through helium-leak-tight graphene-based membranes. *Science* **335,** 442–444 (2012).
13. Leenaerts, O., Partoens, B. & Peeters, F. M. Graphene: a perfect nanoballoon. *Appl. Phys. Lett.* **93,** 193107 (2008).
14. Chen, S. *et al.* Oxidation resistance of graphene-coated Cu and Cu/Ni alloy. *ACS Nano* **5,** 1321–1327 (2011).
15. Ozeki, S., Ito, T., Uozumi, K. & Nishio, I. Scanning tunneling microscopy of UV-induced gasification reaction on highly oriented pyrolytic graphite. *Jpn. J. Appl. Phys.* **35,** 3772–3774 (1996).

16. Huh, S. *et al.* UV/ozone-oxidized large-scale graphene platform with large chemical enhancement in surface-enhanced Raman scattering. *ACS Nano* **5,** 9799–9806 (2011).
17. Novoselov, K. S. *et al.* Two-dimensional atomic crystals. *Proc. Natl Acad. Sci. USA* **102,** 10451–10453 (2005).
18. Koenig, S. P., Boddeti, N. G., Dunn, M. L. & Bunch, J. S. Ultrastrong adhesion of graphene membranes. *Nature Nanotech.* **6,** 543–546 (2011).
19. Liu, L. *et al.* Graphene oxidation: thickness-dependent etching and strong chemical doping. *Nano Lett.* **8,** 1965–1970 (2008).
20. Chang, H. & Bard, A. J. Scanning tunneling microscopy studies of carbon–oxygen reactions on highly oriented pyrolytic graphite. *J. Am. Chem. Soc.* **113,** 5588–5596 (1991).
21. Bieri, M. *et al.* Porous graphenes: two-dimensional polymer synthesis with atomic precision. *Chem. Commun.* 6919–6921 (2009).
22. Girit, C. O. *et al.* Graphene at the edge: stability and dynamics. *Science* **323,** 1705–1708 (2009).
23. Schrier, J. Fluorinated and nanoporous graphene materials as sorbents for gas separations. *ACS Appl. Mater. Interf.* **3,** 4451–4458 (2011).
24. Bai, J., Zhong, X., Jiang, S., Huang, Y. & Duan, X. Graphene nanomesh. *Nature Nanotech.* **5,** 190–194 (2010).
25. Sint, K., Wang, B. & Král, P. Selective ion passage through functionalized graphene nanopores. *J. Am. Chem. Soc.* **130,** 16448–16449 (2008).
26. Fan, Z. *et al.* Easy synthesis of porous graphene nanosheets and their use in supercapacitors. *Carbon* **50,** 1699–1703 (2012).
27. Fox, D. *et al.* Nitrogen assisted etching of graphene layers in a scanning electron microscope. *Appl. Phys. Lett.* **98,** 243117 (2011).
28. Breck, D. W. in *Zeolites Molecular Sieves: Structure, Chemistry, and Use* 593–724 (Wiley, 1973).
29. Bunch, J. S. *et al.* Electromechanical resonators from graphene sheets. *Science* **315,** 490–493 (2007).
30. Hencky, H. Uber den spannungzustand in kreisrunden platten mit verschwindender biegungssteiflgeit. *Z. fur Mathematik und Physik* **63,** 311–317 (1915).
31. Blakslee, O. L., Proctor, D. G., Seldin, E. J., Spence, G. B. & Weng, T. Elastic constants of compression-annealed pyrolytic graphite. *J. Appl. Phys.* **41,** 3373–3382 (1970).

Author contributions

S.P.K. and L.W. performed the experiments. S.P.K. and J.S.B. conceived and designed the experiments. All authors interpreted the results and co-wrote the manuscripts.

Additional information

Supplementary information is available in the online version of the paper. Reprints and permission information is available online at http://www.nature.com/reprints. Correspondence and requests for materials should be addressed to J.S.B.

Competing financial interests

The authors declare no competing financial interests.